Colloid transport in unsaturated porous media: The role of water content and ionic strength on particle straining

Saeed Torkzaban [a], Scott A. Bradford [b,*],
Martinus Th. van Genuchten [b], Sharon L. Walker [a]

[a] *Department of Chemical and Environmental Engineering, University of California, Riverside, CA 92521, United States*
[b] *US Salinity Laboratory, USDA-ARS, 450 W. Big Springs Road, Riverside, CA 92507-4617, United States*

Abstract

Packed column and mathematical modeling studies were conducted to explore the influence of water saturation, pore-water ionic strength, and grain size on the transport of latex microspheres (1.1 µm) in porous media. Experiments were carried out under chemically unfavorable conditions for colloid attachment to both solid–water interfaces (SWI) and air–water interfaces (AWI) using negatively charged and hydrophilic colloids and modifying the solution chemistry with a bicarbonate buffer to pH 10. Interaction energy calculations and complementary batch experiments were conducted and demonstrated that partitioning of colloids to the SWI and AWI was insignificant across the range of the ionic strengths considered. The breakthrough curve and final deposition profile were measured in each experiment indicating colloid retention was highly dependent on the suspension ionic strength, water content, and sand grain size. In contrast to conventional filtration theory, most colloids were found deposited close to the column inlet, and hyper-exponential deposition profiles were observed. A mathematical model, accounting for time- and depth-dependent straining, produced a reasonably good fit for both the breakthrough curves and final deposition profiles. Experimental and modeling results suggest that straining — the retention of colloids in low velocity regions of porous media such as grain junctions — was the primary mechanism of colloid retention under both saturated and unsaturated conditions. The extent of stagnant regions of flow within the pore structure is enhanced with decreasing water content, leading to a greater amount of retention. Ionic strength also contributes to straining, because the number of colloids that are held in the secondary energy minimum increases with ionic strength. These weakly associated colloids are prone to be translated to stagnation regions formed at grain–grain junctions, the solid–water–air triple point, and dead-end pores and then becoming trapped.
Published by Elsevier B.V.

Keywords: Colloid transport; Deposition; Straining; Ionic strength; Hydrodynamics

1. Introduction

Colloid movement through porous media is of great significance in a number of environmental fields including contaminant transport, soil profile development, and subsurface migration of pathogenic microorganisms. Pathogenic microorganisms such as bacteria and viruses

---

* Corresponding author. Tel.: +1 951 369 4857; fax: +1 951 342 4963.
  E-mail address: sbradford@ussl.ars.usda.gov (S.A. Bradford).

(often referred to biocolloids) pose a high risk to water resources through land application of raw and treated wastewater, septic systems, leaking sewage pipes, and animal manure (Hurst, 1980; Powelson et al., 1993; Redman et al., 2001). Colloid transport in porous media is also of concern due to colloid-facilitated transport of a wide variety of inorganic and organic contaminants that adsorb onto these particles and travel significant distances (de Jonge et al., 1998; Ryan et al., 1998; McGechan and Lewis, 2002). Hence, comprehensive knowledge of the transport of colloidal particles in subsurface environments is essential for predicting biological and chemical contaminant fate. Considerable research has been devoted to the fate and transport of colloids in saturated porous media (reviews are given by Schijven and Hassanizadeh, 2000; Harvey and Harms, 2002; de Jonge et al., 2004); however, colloid transport in the unsaturated (vadose) zone, which often act as a first natural layer against the pollution of groundwater, has received little systematic research and the governing mechanisms are poorly understood.

Mechanisms of colloid retention in unsaturated porous media include adsorption (attachment/detachment processes) to solid–water interfaces (SWI) (reviews are given by Ryan and Elimelech, 1996, Schijven and Hassanizadeh, 2000), air–water interfaces (AWI) (e.g. Wan and Wilson, 1994a), straining (McDowell-Boyer et al., 1986; Bradford et al., 2002, 2003), and film straining (Wan and Tokunaga, 1997; Saiers and Lenhart, 2003a). Attachment to the SWI involves colloid collision with and attachment to grain surfaces, and consequently depends on the chemical and physical characteristics of the colloids and soil surfaces as well as the solution chemistry (Ryan and Elimelech, 1996, Walker et al., 2004). The AWI present within unsaturated porous media is also believed to serve as a collector for colloid particles, reportedly in an irreversible manner, retained by either capillary or electrostatic forces (Wan and Wilson, 1994b; Schafer et al., 1998). Colloid attachment to the AWI, therefore, depends on pH, ionic strength, and colloid surface properties (DeNovio et al., 2004; Torkzaban et al., 2006b). Additionally, Wan and Tokunaga (2002) demonstrated that only positively charged colloidal particles attached at the AWI, and Crist et al. (2004, 2005) observed in three-dimensional porous media that negatively charged-hydrophilic colloids did not attach to the AWI.

Straining involves the retention of colloids in the smallest regions of the pore space (McDowell-Boyer et al., 1986; Cushing and Lawler 1998; Bradford et al., 2002, 2003, 2006a) such as those formed near grain-to-grain contact points. It should be noted that retention of colloids near to grain-to-grain contact points has also been referred to in the literature as wedging (Herzig et al., 1970; Johnson et al., 2007). In the smallest regions of the pore space the water velocity is very low and these locations can be considered as zones of relative flow stagnation. Straining may also occur in pore throats that are too small to allow the passage of multiple colloids (Herzig et al., 1970; Bradford et al., 2002), a process often referred to as bridging (Ramachandran and Fogler, 1999). Criteria for colloid straining in porous media has traditionally been assumed to be simply a function of the ratio of colloid to collector diameters (d_p/d_g) and the pore size distribution of the medium (Herzig et al., 1970; McDowell-Boyer et al., 1986; Bradford et al., 2002, 2003). Herzig et al. (1970) computed that when d_p/d_g exceeds 0.05, straining significantly contributes to retention of colloids in porous media. Recently, a few researchers have suggested that the theoretical criteria of Herzig et al. (1970) underestimates the extent of straining in colloid retention and that straining can be occurring at d_p/d_g as low as 0.002 (Bradford et al., 2002, 2003; Li et al., 2004).

In unsaturated media, straining has received relatively less attention (Gargiulo et al., 2007). In fact, straining may be more pronounced in unsaturated versus saturated porous media because capillary forces constrain water flow within regions having smaller pore spaces. Furthermore, unsaturated systems also contain solid–water–air triple points at the intersection of solid–water and air–water interfaces. Triple points and grain–grain contact points share many similarities in that these locations are both low velocity zones. In this work, we consider retention at the triple point as an additional form of straining. Moreover, the extent to which saturated and especially unsaturated colloid straining is sensitive to changes in the chemical properties of the system (i.e. aqueous phase, colloids, and collectors) remains poorly understood (Bradford et al., 2006a, 2007). In addition to straining, film straining (Wan and Tokunaga, 1997) is another potential retention mechanism needing further investigation. Film straining is the removal of colloids in partially saturated porous media occurring as a result of the physical restrictions to colloid transport through water films with thicknesses smaller than the diameter of the colloids.

Previous studies on unsaturated colloid transport have mainly focused on the determination of the colloid concentration in the effluent (e.g. Saiers and Lenhart, 2003a; Torkzaban et al., 2006a,b). Breakthrough concentrations are typically simulated by using a variety of parameters to best fit the data that consider SWI and/or AWI adsorption rate coefficients, and/or film straining coefficients. Few studies have reported the shape of the

colloid deposition profiles for unsaturated conditions. Bradford et al. (2003) demonstrated in saturated colloid transport experiments that breakthrough curves can be adequately fit using a variety of models such as an attachment and detachment model, or an attachment and straining model. The study showed that consideration of both breakthrough curves and deposition profiles in model fitting is vital to gain insight on the controlling deposition mechanisms.

The objective of this work was to explore the effects of water content and solution ionic strength on colloid transport and retention. Highly unfavorable attachment conditions were employed to ensure a high repulsive energy barrier against attachment and therefore the retention mechanisms involved were not attachment by simply chemical interactions, but rather by straining. To minimize colloid attachment to both the SWI and AWI, the experiments were conducted using hydrophilic, negatively charged microspheres in a buffered solution such that the SWI and AWI were negatively charged. Unfavorable attachment conditions were confirmed to exist through complementary batch experiments and DLVO calculations. The breakthrough data and final deposition profile were measured and simulated using the HYDRUS-1D code that accounts for time and depth-dependent deposition processes. Fitted model parameters were used to gain insight into the various mechanisms controlling colloid transport in unsaturated systems.

2. Materials and methods

2.1. Tracer, colloid, and sand materials

The background electrolyte solution utilized in this study consisted of deionized water buffered to pH 10 (1.67 mM $NaHCO_3 + 1.67$ mM Na_2CO_3). Sodium nitrate (0.2 mM, Fisher Scientific) was used as a conservative tracer to characterize the hydrodynamic properties of the porous medium. Carboxylate-modified latex (CML) colloids (Molecular probes, Inc., Eugene, OR) were selected as model colloid particles. These spherical particles have been employed in previous colloid transport studies reported in the literature (Wan and Wilson, 1994a,b). CML was chosen due to the high density of carboxylic acids on the colloid surface creating a negatively charged-hydrophilic surface. Colloid diameter was 1.1 µm with a particle density (ρ_p) of 1.055 g cm^{-3} and a particle surface charge density (ρ_q) of 0.0175 meq/g. The values of ρ_p and ρ_q were provided by the manufacturer. The concentration of colloid suspension ($2.5–2.8 \times 10^7$ N_c ml^{-1}; where N_c denotes number of colloids) was selected to minimize any permeability reductions of the porous medium.

Two different sizes of Ottawa aquifer sand (U.S. Silica, Ottawa, IL) were used in this study. These sands are designated hereafter as 3550 and MIX having median grain sizes (d_{50}) of 360 and 240 µm, respectively. The uniformity index ($U_i = d_{60}/d_{10}$ where x % of the mass was finer than d_x) of the 3550 and MIX sands was measured to be 1.88 and 3.06, respectively. The capillary pressure–saturation curves for these Ottawa sands were previously reported by Bradford and Abriola (2001). Ottawa sands typically consist of 99.8% SiO_2 (quartz) and trace amounts of metal oxides, are spheroid in shape, and have rough surfaces. Quartz and iron oxides possess a net negative charge at pH 10 (Tipping, 1981; Redman et al., 2004), and any attractive electrostatic interactions between the CML colloids and the porous medium are expected to be minimized at this pH.

2.2. Experimental set-up

The column experiment was designed to accurately establish a steady-state and unit hydraulic gradient along the column in case of unsaturated transport (Fig. 1). A stainless steel column with internal diameter and length of 5 and 10 cm, respectively, was selected for this study. A hydrophilic nylon membrane with 10 µm pore size (SaatiTech, Veniano, Italy), supported by a aluminum end-plate, was used as a capillary barrier at the bottom of the column. The nylon membrane had a bubbling pressure of 70 cm-H_2O. Results of preliminary experiments (performed without sand) demonstrated that neither the column body nor the nylon membrane retained the colloids.

The column was wet-packed with the water level maintained a few centimeters above the sand surface. After the addition of sand, the column was vibrated to ensure a uniform packing and to liberate any trapped air bubbles. Prior to each experiment, the column was flushed upward under saturated conditions with about seven pore volumes of the pH 10 electrolyte solution to free the effluent from background colloids in the sand. The flow was then reversed and the column was rinsed with an additional two pore volumes before starting the transport experiments. The solution chemistry conditions were verified by measuring the pH and ionic strength of the influent and effluent solutions.

A sprinkling apparatus equipped with 7 stainless steel needles was connected to a high performance liquid chromatography (HPLC) pump (Barnant Company, Barrington, IL) and used to evenly distribute the influent over the sand surface. Capillary pressure head was measured with two stainless steel miniature tensiometers (Chemiquip Products Co., West New York, NJ) inserted at 2 and 8 cm from the upper sand surface. Data from the tensiometers
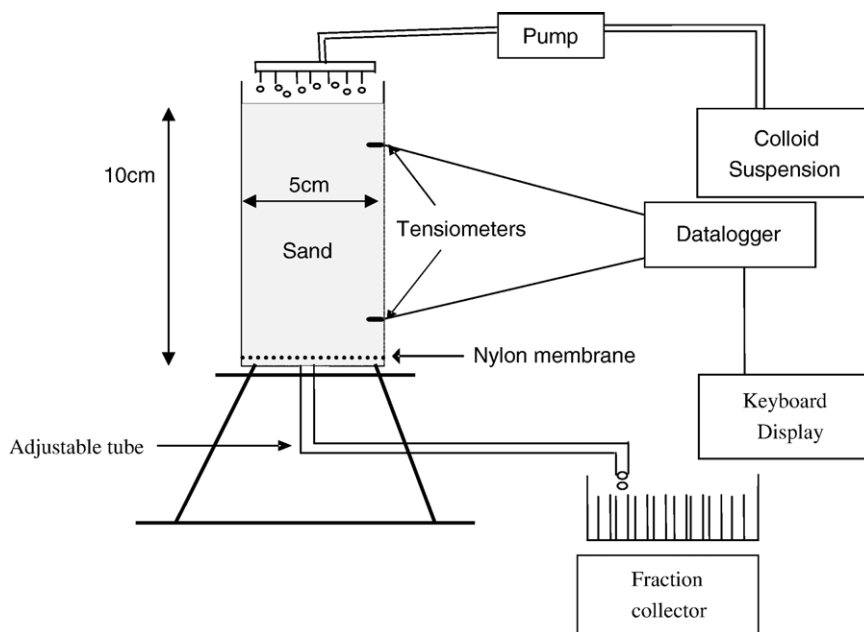
Fig. 1. Schematic representation of the experimental set-up.

were collected continuously using a CR10X datalogger (Campbell Scientific Ltd, Lougborough, UK) and monitored with a keyboard display (CR10KD). The average water content of the column (under steady-state unit gradient flow conditions) was monitored gravimetrically with an electronic balance (Sartorius Master Series, LP Models, Germany) and is listed in Table 1. The lower boundary condition was controlled using a hanging water column to impose a constant suction.

Unsaturated transport experiments involved draining the saturated column to the desired water saturation level by reducing the inflow water rate to the hydraulic conductivity corresponding to that saturation. Simultaneously, the pressure head at the bottom of the column was gradually reduced until the readings of the tensiometers showed the same values. This resulted in a unit hydraulic head gradient, i.e. constant capillary pressure, which implies a constant saturation level along the column. In some experiments, to eliminate the effect of variations in water velocity in our results, a hydraulic gradient was applied in the saturated experiments such that the average water velocity was the same as in the unsaturated experiments. Table 1 indicates the parameters of each column experiment.

2.3. Transport experiment protocol

Column transport experiments were systematically conducted to investigate the transport and deposition behavior of the 1.1 μm CML microspheres under saturated and unsaturated conditions at three different ionic strengths (IS=6, 30, and 60 Mm at a pH of 10). After establishing a specified saturation and water chemistry, transport experiments were carried out in six stages. These stages are described in greater detail below:

Stage 1: Prior to colloid application, tracer experiments were carried out to determine the dispersivity for each saturated condition. A solution

Table 1
Experimental conditions for column experiments in 3550 sand (Li, Mi, and Hi stand for low, medium, and high ionic strength. Lv, Mv, and Hv stand for low, medium, and high velocity)

Exp.	Saturation %	Ionic strength (mM)	Average water velocity (cm/min)	Dispersivity (cm)	Pulse duration (pore volume)
Li100	100	6	0.6	0.08	7.12
Mi100	100	30	0.35	0.08	5.01
Hi100Lv	100	60	0.35	0.08	4.63
Hi100Mv	100	60	0.56	0.08	5.94
Hi100Hv	100	60	0.87	0.08	5.43
Li70	70	6	0.85	0.4	7.08
Mi70	70	30	0.85	0.4	5.09
Hi70	70	60	0.85	0.4	5.51
Li50	50	6	0.6	0.6	7.12
Mi50	50	30	0.6	0.6	5.04
Hi50	50	60	0.6	0.6	5.94
Li40	40	6	0.37	0.8	7.05
Mi40	40	30	0.37	0.8	5.03
Hi40	40	60	0.37	0.8	4.64

containing 0.2 mM NaNO$_3$ was fed into the column at given water saturation and the breakthrough curve was obtained by measuring the absorbance of the effluent at 204 nm using a spectrophotometer (Perkin Elmer LC95 UV/VIS spectrometer, Irvine, CA).

Stage 2: Following the tracer experiment, the influent was switched to the background electrolyte solution in order to flush out the remnant nitrate. This was verified by measuring the absorbance of the effluent. This step also served the purpose of equilibrating the column with the electrolyte to be used in the subsequent colloid transport experiment.

Stage 3: A colloid suspension ($2.5–2.8 \times 10^7$ N_c ml^{-1}) was introduced into the column at a constant rate. The colloid suspension was applied for a given number of pore volumes (pulse duration) as listed in Table 1.

Stage 4: Colloid-free electrolyte solution was applied to the column at the same flow rate until the effluent colloid concentration returned to baseline level. Effluent samples were collected at selected intervals by a fraction collector and analyzed for colloid concentration using a spectrometer (Perkin Elmer LC95 UV/VIS spectrometer, Irvine, CA) at 480 nm.

Stage 5: Following completion of the colloid transport experiments, the spatial distribution of deposited colloids in a sand column was determined (Bradford et al., 2002). The sand was carefully excavated in 1 cm increments and each increment was placed in a 50 mL polypropylene centrifuge tube containing 30 mL of the background electrolyte solution. The tubes were very slowly shaken for a few minutes to liberate reversibly retained colloids. The concentration of colloids in the supernatant solution was measured using a fluorometer (Turner Quantech Fluorometer, Dubuque, IA) following an experimental protocol outlined previously (Bradford et al., 2002). Water and sand were poured into an aluminum dish and placed in an oven for several hours to volatilize all of the remaining water. The volume of water and mass of sand in each tube was determined from mass balance by measuring the weight of the empty tubes, water and sand tubes, and dry sand.

Stage 6: A colloid mass balance was conducted at the end of the column experiment using effluent concentration data and the deposited colloids in the column. The calculated number of effluent and retained colloid particles was normalized by the total number of particles injected into a column.

2.4. Batch experiments

Batch experiments were conducted by placing 10 g of sand and 10 ml of a known initial concentration of colloid suspension into a polypropylene centrifuge tubes with the temperature kept at approximately 20 °C. Three different ionic strength solutions (6, 30, 60 mM) buffered at pH 10, corresponding to the chemical conditions in column experiments, were used for making colloid suspension. The suspension and sand were allowed to equilibrate for 2 h by gently rotating the tubes end over end (15 rpm) on a tube rotator (Fisher Scientific, San Diego, CA). The 2-h equilibration time was chosen to mimic the duration of the column experiments. A control experiment without colloids was also run for measuring the background concentration of colloids introduced from the sand. The initial and final concentrations of colloids in the suspension were determining using the spectrophotometer (Perkin Elmer LC95 UV/VIS spectrometer, Irvine, CA) after setting the tube to rest for a few minutes. All experiments were performed in duplicate.

2.5. Electrokinetic characterization of colloids

The zeta potential of the colloids was measured using a ZetaPals instrument (Brookhaven Instruments Cooperation, Holtsville, NY). The measurements were carried out three times for each condition and the average values were -110, -85, -71 mV for the colloids suspended in 6, 30, and 60 mM ionic strength solutions, respectively. The AWI has been reported to be negatively charged over a very wide range of ionic strength and pH (Li and Somasundaran, 1991; Gracia et al., 1995). According to results obtained by Li and Somasundaran (1991), the zeta potential of air bubbles in NaCl solution at pH 10 and a solution ionic strength with a range of 0.01–100 mM varies from -90 to -50 mV. The zeta potential of quartz sand surfaces in pH 10 solution has been reported previously to be approximately -70 mV (Elimelech et al., 2000). These values were used in calculations for electrostatic forces presented later in this paper.

3. Colloid transport model for saturated and unsaturated systems

The HYDRUS-1D code (Simunek et al., 2005) is a finite element model for simulating the one-dimensional movement of water, heat, and multiple solutes in variably saturated media. The code numerically solves the

Richards' equation for saturated–unsaturated water flow and Fickian-based advection–dispersion equations for the non-linear equilibrium and kinetic reactions between colloids and the SWI. The code is coupled to a non-linear least square optimization routine based upon the Levenberg–Marquardt algorithm (Marquardt, 1963) to fit model parameters to breakthrough curve and/or deposition profile information. Relevant aspects of the code that were used to simulate the colloid transport data are described below.

The transport of colloids through the sand columns was described using the one-dimensional form of the advection–dispersion equation (ADE) that accounts for colloid deposition in the column:

$$\frac{\partial C}{\partial t} = \lambda v \frac{\partial^2 C}{\partial z^2} - v \frac{\partial C}{\partial z} - r_d \qquad (1)$$

where C is the number of colloids per unit volume of the aqueous phase ($N_c\,L^{-3}$), λ is the dispersivity (L), v is the average pore-water velocity (LT^{-1}), and r_d is the mass transfer rate of colloids in aqueous phase to/from the deposited phase ($N_c\,L^{-3}T^{-1}$) given by:

$$\rho_b \frac{\partial S_d}{\partial t} = r_d = \theta K_d \psi_s C - \rho_b K_{det} S_d \qquad (2)$$

where ρ_b is the soil bulk density (ML^{-3}), θ is the volumetric water content (−), K_d is the colloid deposition coefficient (T^{-1}), ψ_s is a dimensionless deposition function for deposited colloids (−), S_d is the concentration of deposited colloids in the column ($N_c\,M^{-1}$), and K_{det} is the first-order detachment rate coefficient (T^{-1}).

A simple and flexible form for ψ_s is used in the model to account for time and depth-dependent deposition behavior as (Bradford et al., 2003):

$$\psi_s = \left(1 - \frac{S_d}{S_{max}}\right)\left(\frac{d_{50} + z}{d_{50}}\right)^{-\beta} \qquad (3)$$

where d_{50} is the median grain size of the porous medium (L), β is a parameter that accounts for the spatial distribution of retained colloids (−), S_{max} is the maximum concentration of deposited colloids ($N_c\,M^{-1}$), and z is the down gradient distance from the porous medium inlet (L). The first term on the right hand side of this equation is used to account for time-dependent deposition in a manner similar to Langmuirian blocking (Adamczyk et al., 1994). When the value of S_{max} is large then this term approaches a value of 1 and time-dependent deposition behavior becomes irrelevant. The second term on the right hand side of the above equation is used to describe depth-dependent deposition behavior; i.e., hyper-exponential profiles with decreasing deposition rates with increasing

depth. When β goes to zero, then depth-dependent deposition is not considered. Bradford et al. (2003) reported that the value of $\beta = 0.432$ gave a good description of the spatial distribution of retained colloids when significant straining occurred; hence this value was used in the simulations reported in this paper.

Based on the theoretical approach presented above, mechanisms of colloid deposition such as straining, film straining, and attachment to the SWI and AWI are lumped together in a single exchange term, r_d. Below we present experimental evidence to help identify the relative importance of each of these deposition mechanisms for our experimental conditions, and to provide more evidence for our model formulation.

4. Results and discussion

4.1. Tracer experiments

Breakthrough curves for the conservative tracer under both saturated and unsaturated conditions were well-described by the classical ADE (Eq. (1)). Fig. 2 shows an observed and ADE-simulated nitrate breakthrough curve in 3550 sand at 50% water saturation. Other nitrate breakthrough curves for unsaturated systems gave similar results. Tables 1 and 2 report the value of dispersivity obtained by fitting the experimental data with the HYDRUS-1D model. The dispersivity values
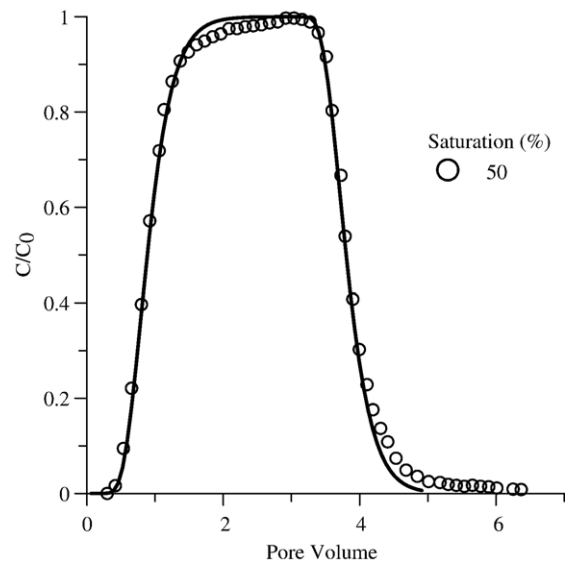
Fig. 2. Measured (symbols) and fitted (lines) breakthrough curves of the tracer (NaNO$_3$) in an experiment carried out in 3550 sand at 50% water saturation.

Table 2
Experimental conditions for column experiments in MIX sand (Li, Mi, and Hi stand for low, medium, and high ionic strength)

Exp.	Saturation	Ionic strength (mM)	Average water velocity (cm/min)	Dispersivity (cm)	Pulse duration (pore volume)
Li100	100	6	0.28	0.1	3.8
Mi100	100	30	0.39	0.1	2.7
Hi100	100	60	0.56	0.1	5.4
Li80	80	6	0.35	0.22	3.3
Mi80	80	30	0.35	0.22	3.0
Hi80	80	60	0.35	0.22	4.2
Li60	60	6	0.23	0.5	3.5
Mi60	60	30	0.23	0.5	2.8

increase with decreasing water content similar to what has been reported in the literature (Toride et al., 2003). Fig. 2 also demonstrates that the tracer exhibits small amounts of tailing in the declining limb of the breakthrough curve under unsaturated conditions. Similar, breakthrough tailing behavior has also been reported in literature (Padilla et al., 1999; Toride et al., 2003), and is believed to occur as a result of immobile regions (inaccessible to flow) existing in unsaturated porous media. Although the physical non-equilibrium model, which accounts for both mobile and immobile regions, can provide a superior description to the tracer breakthrough curve than the simple advection–dispersion model (Cherrey et al., 2003), we decided to utilize the ADE model to be consistent with subsequent colloid transport modeling. We do believe, however, that immobile regions may play an important role on colloid transport and this will be discussed in greater detail later on in the paper.

4.2. Colloid transport

Figs. 3–5 present measured and fitted breakthrough curves for column experiments conducted with varying water contents and solution ionic strengths in 3550 (Figs. 3a–b and 4a–c) and MIX (Fig. 5a–c) sands, respectively. In these figures the normalized effluent concentration is plotted versus the number of pore volumes passed through the column. After approximately 1 pore volume, the injected colloids break through the column and are detected in the effluent. The influent was switched to a colloid-free solution after a given number of pore volumes listed in Tables 1 and 2. For both sands, lower water contents tended to result in lower peak effluent concentrations and greater colloid retention (see Figs. 3a–b, 4a–c, 5a–c, and Tables 3 and 4). However, this effect was more pronounced with increasing ionic

strength. For each water content and sand combination, increasing the ionic strength resulted in lower peak effluent concentrations, indicating greater retention of colloids.

The breakthrough curves shown in Fig. 4 (a–c) obtained in the experiments conducted with 3550 sand and ionic strength of 60 mM indicate that average water velocity also has a significant effect on the colloid retention. The mass recovery in the effluent decreased from 52% to 23% when the average water velocity decreased from 0.87 to 0.35 cm/min, as shown in Tables 3 and 4. All of the breakthrough curves for colloids exhibited an increasing trend: i.e. during the period of continued colloid addition, the effluent concentration increased with time. This suggests the
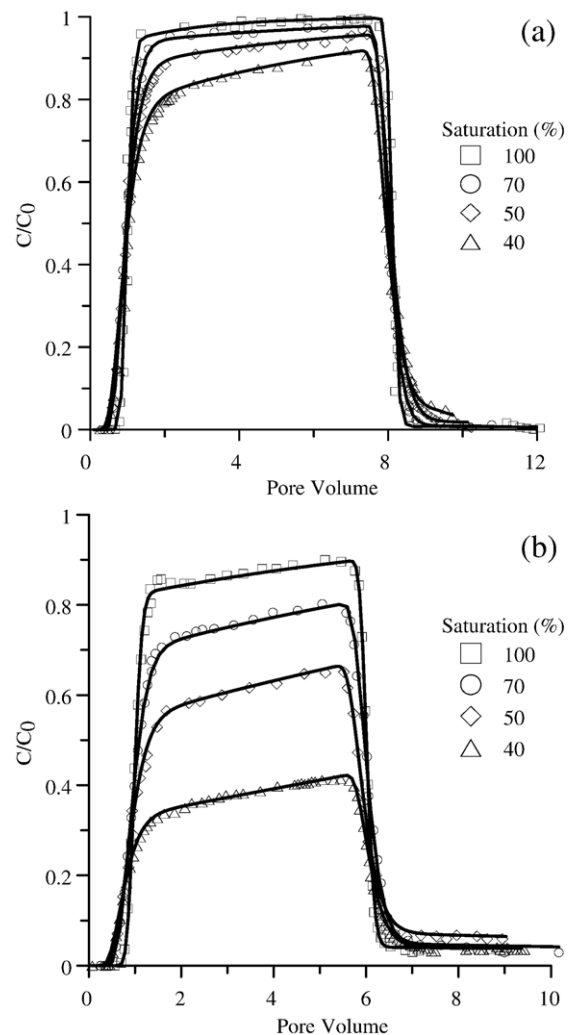

Fig. 3. Observed and simulated breakthrough curves of colloids for various saturation levels in 3550 sand at an ionic strength of 6 mM (a) and 30 mM (b).
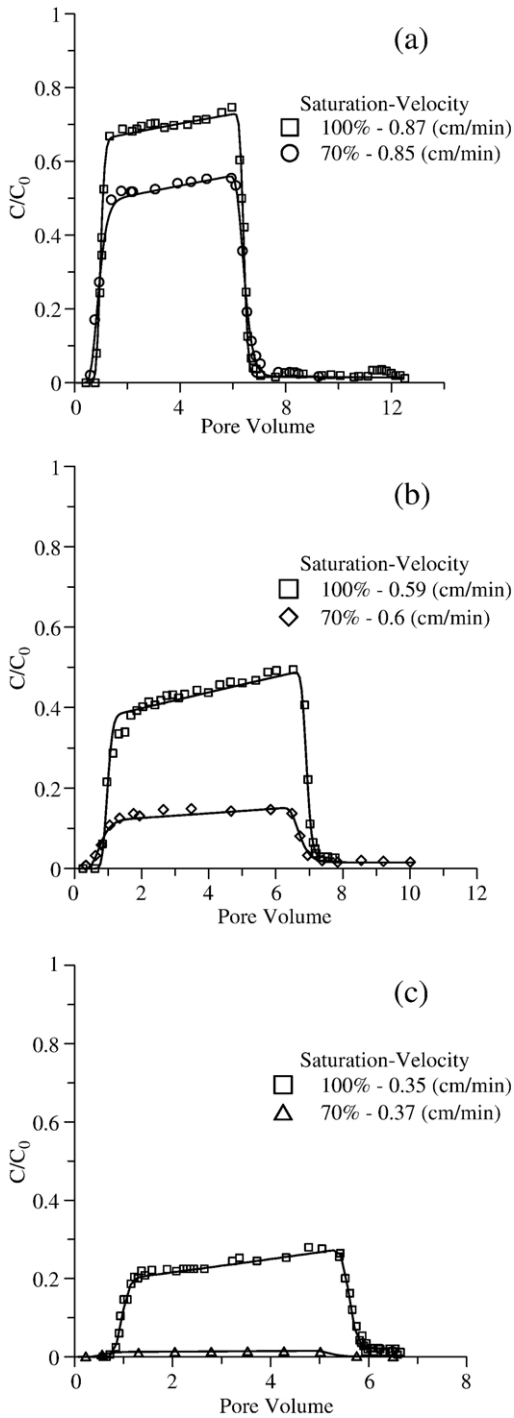
Fig. 4. Observed and simulated breakthrough curves of colloids for various saturation levels in 3550 sand at an ionic strength of 60 mM. The average water velocity was approximately the same in saturated and unsaturated conditions.

filling of deposition sites occurred with time. The apparent tailing behavior of the breakthrough curves implies a low detachment rate of retained colloids.

Figs. 6a–d and 7a–b present the observed and simulated colloid deposition profiles at various water saturation levels and IS in 3550 (Fig. 6a–d) and MIX
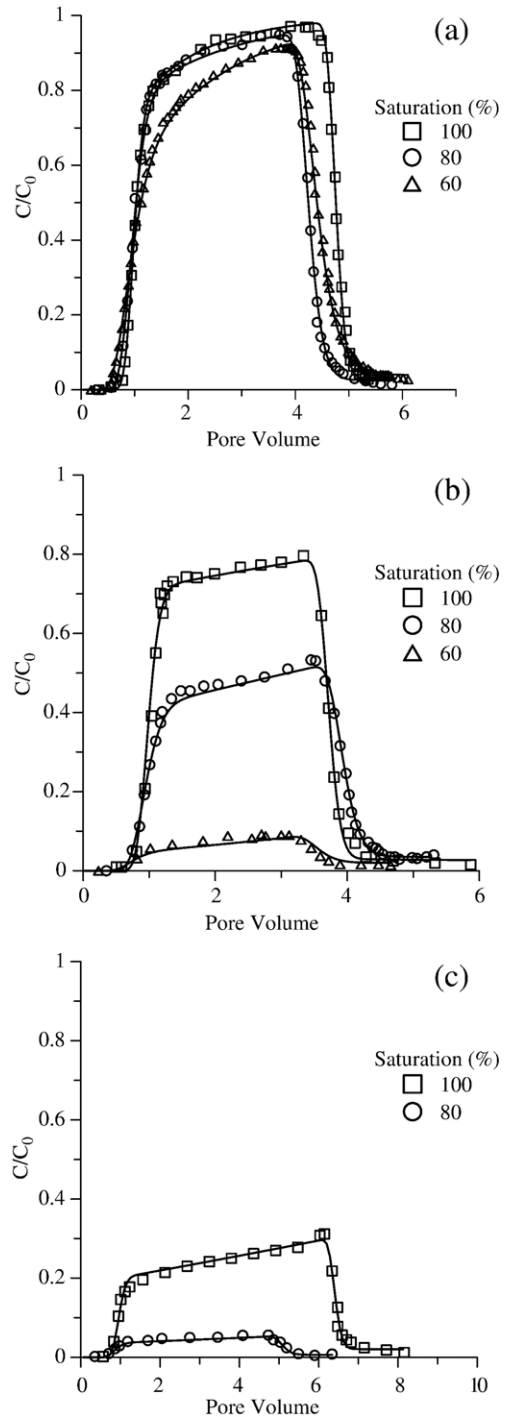

Fig. 5. Observed and simulated breakthrough curves of colloids for various saturation levels in MIX sand at an ionic strength of 6 mM (a), 30 mM (b), and 60 mM (c).

Table 3
Fitted model parameters in 3550 sand and various solution ionic strengths

Exp.	S_{max}* (g^{-1})	K_d (min^{-1})	K_{det} (min^{-1})	M_E	M_S	M_T	R^2
Li100	0.03	0.01	0.004	98	N.m [a]	>98	98
Mi100	0.65	0.019	0.0024	87.6	11.7	99.3	99
Hi100Hv	1.8	0.1	0.001	53	52	105	97
Hi100Mv	3.6	0.16	0.0008	32	55	87	97
Hi100Lv	5.5	0.26	0.0005	23	67	90	98
Li70	0.07	0.015	0.003	97	N.m	>97	97
Mi70	0.74	0.084	0.004	78	20	98	96
Hi70	2.5	0.17	0.0008	54	44	98	97
Li50	0.1	0.02	0.0024	93	N.m	>93	94
Mi50	1.3	0.1	0.003	66	22	88	96
Hi50	8.4	0.39	0.00063	22	75	97	97
Li40	0.16	0.024	0.002	87	N.m	>87	97
Mi40	1.8	0.13	0.0008	38	61	99	96
Hi40	12	0.6	0.0002	1.5	86	87.5	95

Also included in this table are the effluent (M_E), sand (M_S), and the total (M_T) mass percentage recovered for the experimental systems and the coefficient of linear regression. The parameter S_{max}*$=S_{max}/N_{ic}$; where N_{ic} in the number of colloids in a unit volume of influent suspension.

[a] N.m: Not measured.

(Fig. 7a–b) sands, respectively. The data are presented here as normalized concentration (number of colloids recovered in the sand, N_c, divided by the total number of colloids injected into the column, N_{ct}) per gram of dry sand and are plotted as a function of distance from the column inlet. The data indicate that the highest retention occurred near to the column inlet and that the profile shape was hyper-exponential with depth.

Consistent with the breakthrough curves, Tables 3 and 4 indicates that the percent recovery of colloids in the sands enhanced with decreasing water content and increasing ionic strength. The total percent recovery for colloids in the effluent and sands ranged from 87–105% (Tables 3 and 4). This signifies that most of retained colloids in the column were recovered — either by elution or simply resuspension of the sand after the column experiments.

4.3. Application of HYDRUS-1D model

To quantitatively compare the experiments, breakthrough and deposition data were simulated by fitting with the solutions of Eqs. (1) and (2). Tables 3 and 4 summarize the fitted parameters and R^2 values for all column experiments. Application of the transport and deposition model produced a good fit to the breakthrough data with R^2 values close to one as seen in Tables 3 and 4 for all of the experiments conducted. For both sand sizes, the values of K_d and S_{max} increased with ionic strength. The same behavior for K_d and S_{max} was observed for decreasing water content but it was

more pronounced in higher ionic strength solutions. The values of K_{det} in Tables 3 and 4 were typically several orders of magnitude lower than K_d. It can also be observed in Figs. 6a–d and 7a–b that this model predicted the deposition profile behavior reasonably well.

4.4. Batch experiments and DLVO calculations

Batch experiments were conducted to determine the potential for colloid attachment to the sand without the influence of pore structure. These experiments were conducted under a range of selected experimental conditions (20 °C, pH=10, ionic strength=6, 30, and 60 mM), and were consistent with unfavorable conditions for attachment. The difference between the initial and final concentrations of colloids in solution was less than 1%. This suggests that the presence of any chemical heterogeneity on the quartz sands had negligible effect on irreversible colloid attachment.

To better understand the chemical interactions between colloids and the SWI the total interaction energy was calculated using the classic Derjaguin–Landau–Verwey–Overbeek (DVLO) theory (Derjaguin, 1954). In this case, the total interaction energy consists of the sum of attractive van der Waals (Gregory, 1981) and repulsive electrostatic (Hogg et al., 1966) interactions, and was approximated as a sphere-plate interaction. Zeta potential values were used in the place of surface potential values in the DLVO calculations, and the Hamaker constant for the carboxylate-modified latex (CML) colloids–water–sand system was set equal to 4.04×10^{-21} (Bergendahl and Grasso, 1999). As noted earlier, the measured zeta potential of the colloids becomes less negative with increasing ionic strength which is due to compression of the electrostatic double layer. The same behavior is likely for both the AWI and SWI; however for purposes of

Table 4
Fitted model parameters in MIX sand and various solution ionic strengths

Exp.	S_{max}* (g^{-1})	K_d (min^{-1})	K_{det} (min^{-1})	M_E	M_S	M_T	R^2
Li100	0.075	0.024	0.003	92	N.m [a]	>92	92
Mi100	0.78	0.042	0.002	77.6	19.2	96.8	97
Hi100	5	0.29	0.0006	25	63	88	93
Li80	0.08	0.027	0.003	91	N.m	>91	94
Mi80	1.5	0.1	0.0012	49	55	104	98
Hi80	11	0.4	0.0004	5	82	87	97
Li60	0.09	0.035	0.002	86	N.m	>86	98
Mi60	2.7	0.26	0.001	9	94	103	96

Also included in this table are the effluent (M_E), sand (M_S), and the total (M_T) mass percentage recovered for the experimental systems and the coefficient of linear regression. The parameter S_{max}*$=S_{max}/N_{ic}$; where N_{ic} in the number of colloids in a unit volume of influent suspension.
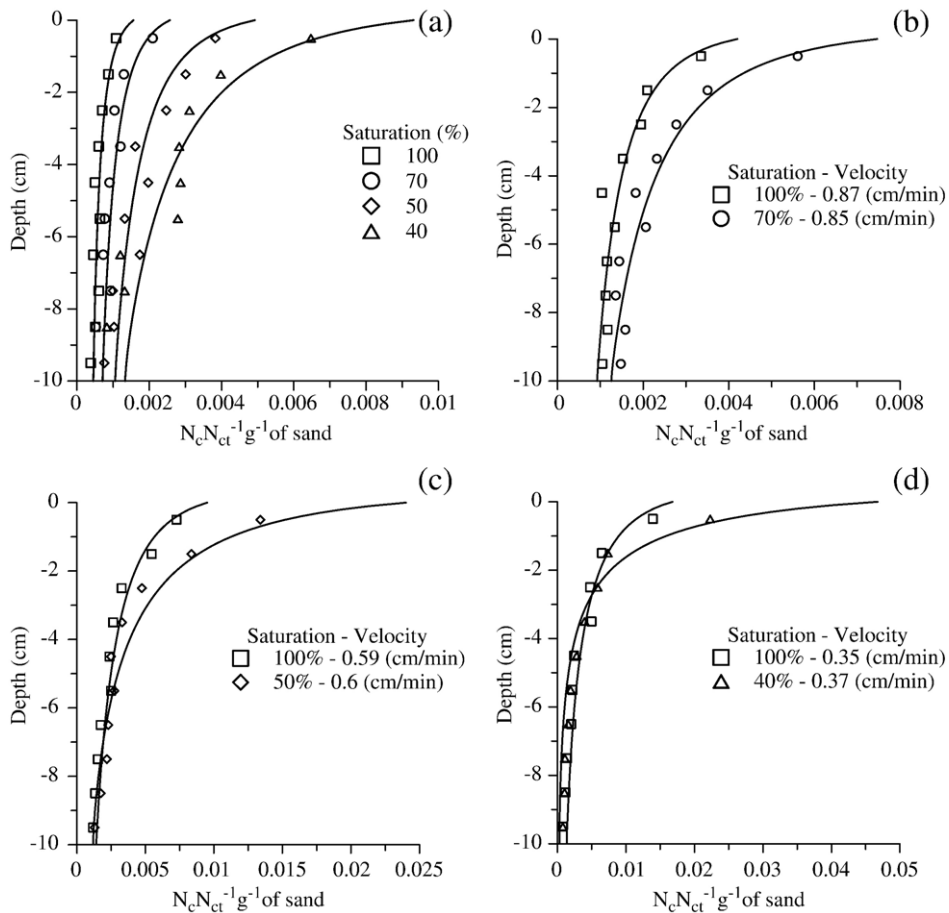
[a] N.m: Not measured.

Fig. 6. Observed and simulated deposition profiles of colloids for various saturation levels in 3550 sand at an ionic strength of 30 mM (a) and 60 mM (b–d). The average water velocity was the same in saturated and unsaturated conditions in experiments conducted at an ionic strength of 60 mM.

DLVO calculations, we assumed these values to be constant over the range of ionic strengths. Fig. 8 presents the total interaction energy between the colloids and quartz surface upon close approach over the range of solution chemistry conditions tested in transport experiments. These calculations indicate the presence of a significant energy barrier to attachment in the primary energy minimum and a shallow secondary energy minimum at greater distance from the SWI. The depth of the secondary energy minimum increases with ionic strength ranging from 0.3 kT at 6 mM to 2.9 kT at 60 mM, with corresponding separation distances of 46 to 10 nm, respectively. Note that k is the Boltzmann constant and T is the temperature in degrees Kelvin. These DLVO calculations corroborate with the batch experiment finding that there is a negligible amount of colloid adsorption to sand particles.

Similar DLVO calculations were also made to predict the interaction energy between the CML colloids and the AWI. As noted earlier, the zeta potential of the colloids and the AWI is negative resulting in a repulsive electrostatic interaction between the colloids and AWI. In contrast with the SWI, the value of the Hamaker constant for the AWI-CML colloids–water system is negative (-1.2×10^{-20} J; e.g. see Israelachvili, 1992) leading to a repulsive van der Waals interaction for these colloids as they approach the AWI. Hence, colloid attachment to the AWI is predicted to be even less favorable for the AWI than for the SWI.

4.5. Implications for colloid transport and retention

Experimental evidence in this study has demonstrated that attachment to the SWI is not the dominant mechanism responsible for colloid retention. The first piece of indirect evidence is the batch experiments which found no significant colloid attachment to the sand. Additionally, the experimental protocol for
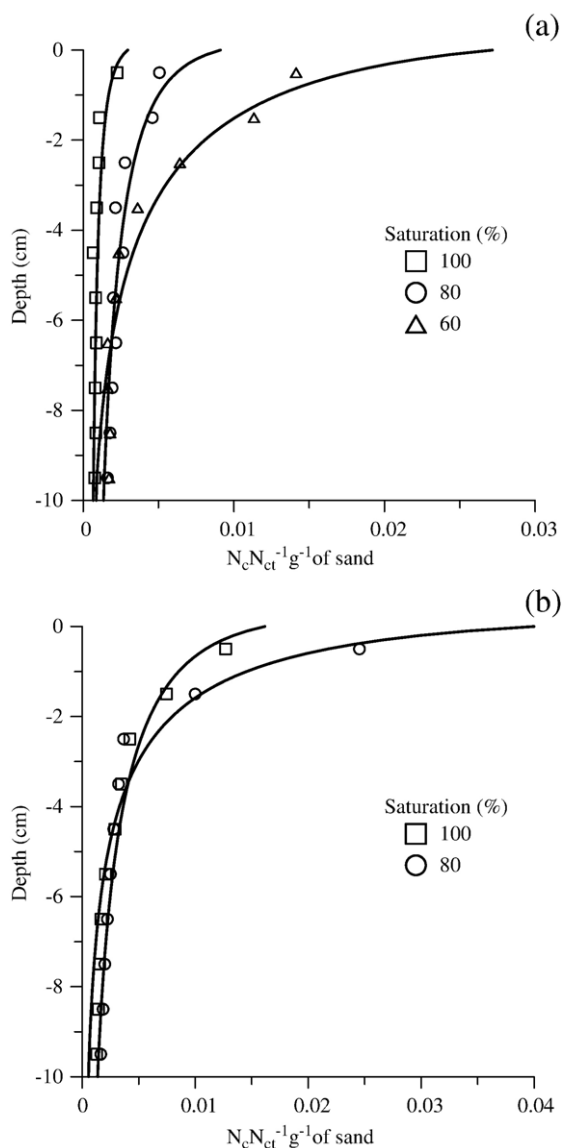
Fig. 7. Observed and simulated deposition profiles of colloids for various saturation levels in MIX sand at an ionic strength of 30 mM (a) and 60 mM (b).

barrier against colloid attachment. Finally, the colloid deposition profiles resulting from the column experiments were not consistent with first-order attachment–detachment model predictions. Specifically, the value of β (Eq. (3)) was greater than zero, indicating depth-dependent deposition rather than first-order attachment.

Non-exponential deposition profiles under saturated conditions have been attributed to charge variability of the porous medium (Johnson and Elimelech, 1995), heterogeneity in colloid surface charge characteristics (Bolster et al., 1999; Li et al., 2004), and deposition of colloids in a secondary energy minimum (Redman et al., 2004; Tufenkji and Elimelech, 2005b). These factors may be involved; however, these mechanisms cannot fully explain the experimental data presented in this paper. The experiments were conducted in a solution at a pH 10, which should minimize any effect of charge heterogeneity on the sand surface because the isoelectric points of most metal oxides fall below this pH (Elimelech et al., 2000). The results of our batch experiments do not support the existence of any significant heterogeneity on the grain or colloid surfaces. Furthermore, the colloids may be held in secondary minima; however, this cannot explain the observed depth- and grain size-dependent deposition. Therefore, another retention mechanism must also be involved.

Retention of colloids under unsaturated conditions has also been attributed to partitioning at the AWI and/or film straining (e.g. Wan and Wilson 1994a; Wan and Tokunaga 1997; Lenhart and Saiers, 2002; Saiers and Lenhart, 2003a). However, attachment to the AWI is not believed to play a significant role in the reported unsaturated experiments, as both the AWI and colloids
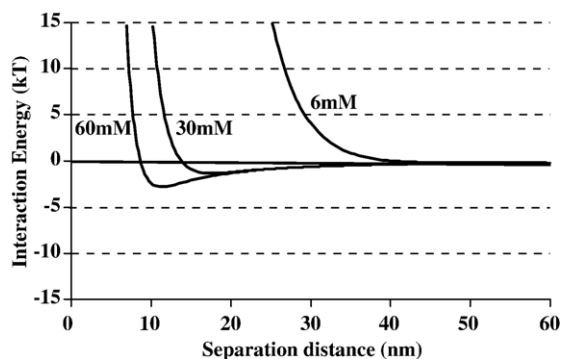
determining the deposition profiles was based upon the rapid release of colloids into solutions, and the high recoveries were not consistent with the low detachment rates that were observed in the column experiments. If the colloids were irreversibly attached to the SWI, they should have remained on the grain surface even after suspending the sand in the same solution that was used for the transport experiments. The next piece of evidence is the fact that colloid retention occurred in the column, even under conditions when DLVO calculations indicate the presence of a substantial energy

Fig. 8. Calculated DLVO interaction energies for 1.1 µm CML colloids as a function of separation distance and ionic strength (indicated next to each curve). Interaction energies were calculated using the zeta potentials in the place of surface potentials. The Hamaker constant for the colloid–water–sand media was assumed to be 4.04×10^{-21} J (Bergendahl and Grasso, 1999).

were negatively charged even in the highest ionic strength solution (see Table 2) and the van der Waals interaction was repulsive. It has been well documented that hydrophilic-negatively charged colloids are unlikely to attach to the negatively charged AWI (e.g. Wan and Tokunaga 2002; Crist et al., 2004, 2005; Torkzaban et al., 2006a, 2006b). Torkzaban et al. (2006a) investigated viral transport under a range of water saturation levels at pH 9 and reported no retention of viruses in the unsaturated columns. Crist et al. (2004, 2005) visually demonstrated that hydrophilic latex colloids did not adsorb on the AWI using a real-time pore-scale microscopic method.

It is also unlikely that film straining plays a major role in the reported colloid retention as the l.1 µm latex colloids are too large to be bound within a thin film. These thin water films have calculated thicknesses around 50 nm during steady-state water flow over an order of magnitude thinner than the diameter of the colloids used in this study (Zevi et al., 2005). Moreover, film straining is theoretically independent of solution ionic strength and flow velocity (Wan and Tokunaga, 1997). In contrast, notably more colloid retention is observed in higher ionic strength solutions and for lower water velocities.

Straining of colloids provides a plausible explanation and mechanism for the observed colloid deposition behavior. Strained colloids become trapped in the smallest regions of the pore space where the flow velocity is reduced. These nearly immobile regions (Patzek and Silin, 2001; Patzek and Kristensen, 2001) include the small pore spaces formed at grain-to-grain contacts, dead-end pores, and the three-phase contact line of the solid–water–air interface (in case of unsaturated conditions). Fluorescent microscopy and X-ray microtomography studies have demonstrated that colloids accumulate in the narrow region of the pore spaces near the contacts of irregularly shaped sand grains under unfavorable attachment conditions (Bradford et al., 2005, 2006a; Xu et al., 2006; Li et al., 2006; Yoon et al., 2006). In these studies, pore-space constrictions apparently served as locations for colloid retention by straining, whereas few colloids appeared to be immobilized far from the grain-to-grain contacts. Colloid retention in the pore network is further supported by Hoek and Agarwal (2006) who reported that DLVO forces act on colloids up to 5 times more in small pore spaces (surface roughness) than with a single flat surface. Straining, as the mechanism of colloid retention, is also supported by mass balance calculations and the fact that once the sand is resuspended in the solution and the pore structure eliminated, the colloids return to solution.

Straining has recently been demonstrated to be a strong function of DLVO and hydrodynamic forces (Bradford et al., 2006a; Bradford et al., 2007). Colloids that are weakly associated with the SWI via the secondary energy minima experience significant hydrodynamic forces (e.g. fluid drag, lift forces) due to fluid flow. The shear force acting on the colloid surface held in the secondary energy minimum is different than that acting on the colloid surface in the bulk fluid. Consequently, at close range to the SWI the colloids experience a combination of forces (hydrodynamic forces, electrical double-layer repulsion, and London-van der Waals) that creates a torque and hence rotation on the surface. (Cushing and Lawler 1998; Bergendahl and Grasso 2000). It has been proposed that weakly associated colloids with the SWI via the secondary energy minimum can be translated and/or funneled by these fluid drag forces to low velocity regions of the pore structure or "straining sites" (Bradford et al., 2007). Indeed, recent experimental evidence by Kuznar and Elimelech (2007) demonstrates that colloids captured in the secondary energy minimum can be translated along the collector surface via hydrodynamic forces and be retained in low velocity regions. Based on this argument, more colloids will be retained in a secondary energy minimum as the ionic strength is increased and these colloids will subsequently be funneled to straining sites.

The coupled effects of DLVO and hydrodynamic forces on straining also can explain the observed decrease in colloid retention with increasing fluid velocity. In this case, enhanced hydrodynamic forces may overcome the electrostatic and van der Waals interactions and detach colloids from the grain surface, and thereby minimize the amount of straining. It is also likely that the extent of relatively stagnation regions decreases as the water velocity increases (Patzek and Silin, 2001; Patzek and Kristensen, 2001). This is consistent with our observations and modeling results presented by Cushing and Lawler (1998). In contrast with the column experiments, there is no pore structure in the batch experiments. Therefore, the hydrodynamic shear forces as the result of rotation prevented colloid attachment to the sand grains in the batch experiments.

It was anticipated that the magnitude of straining would be enhanced with decreasing sand size and water saturation level due to greater amount of low velocity regions. Both of these expected trends were verified by our experimental observations. The extent of retention of colloids increased with ionic strength and decreasing soil grain size for all of the various saturation levels tested. This is especially true for the higher ionic strength conditions (Fig. 5b–c) where very little breakthrough of colloids occurred. Comparison of the

breakthrough curves for all of the ionic strength conditions reveals a decrease in peak effluent concentrations with water content. All these results provide substantial direct and indirect evidence that straining is an important removal mechanism for the CML colloids in the Ottawa sands investigated.

The comparison of experimental and modeled results also suggests that straining is the underlying mechanism in colloid deposition in both the saturated and unsaturated systems tested. The concentration of retained colloids enumerated after the column experiments was found to exhibit a hyper-exponential spatial distribution through the length of the column. This indicates the deposition coefficient was depth-dependent, a trend that has previously been associated with straining (e.g., Bradford et al., 2002, 2003, 2006b).

5. Conclusions

Experimental and theoretical studies were conducted to determine the role of solution chemistry and water content on colloid retention under unfavorable attachment conditions. To better understand the underlying mechanism on colloid retention, the experimental conditions were selected to minimize the potential for colloid attachment (solution pH of 10, quartz sands, and highly negatively charged colloids that were hydrophilic). DLVO calculations, mass balance information, and batch experiments confirmed our assumption that attachment to the SWI and AWI was not the dominant mechanism in colloid retention. All the observations discussed above provide convincing evidence that straining was the primary mechanism of colloid retention in our column experiments. The straining rate in a given porous medium is apparently a complicated mechanism, coupled with such parameters as pore size distribution, hydrodynamics, solution chemistry and water content. Specific findings are highlighted below.

- Straining increases in magnitude with increasing ionic strength due to an increased force (secondary energy minimum) and number of colloids that are funneled to and retained in small pores formed adjacent to grain–grain junctions.
- Straining increases in magnitude with decreasing water content due to an increase in the extent of stagnant regions of flow within the pore medium.
- Increasing the flow rate of a system tends to decrease the amount of straining of colloids as a result of the increased fluid drag force that acts on weakly-attached colloids on the SWI and also decreased flow stagnation regions.

- The shape of the colloid deposition profile is highly sensitive to the physical (grain size, water content, and flow rate) and chemical (solution IS and pH) properties of a system due to the interrelation of these parameters on colloid straining.

Additional research is required to better understand and quantify the coupling of physical and chemical processes that influence colloid straining in saturated and unsaturated porous media. This information is believed to be essential for predicting colloid transport and fate in many natural environments.

References

Adamczyk, Z., Siwek, B., Zembala, M., Belouschek, P., 1994. Kinetics of localized adsorption of colloid particles. Adv. Colloid Int. Sci. 48, 151–280.

Bergendahl, J., Grasso, D., 1999. Prediction of colloid detachment in a model porous media: Thermodynamics. AIChE J. 45 (3), 475–484.

Bergendahl, J., Grasso, D., 2000. Prediction of colloid detachment in a model porous media: Hydrodynamics. Chem. Eng. Sci. 55, 1523–1532.

Bolster, C.H., Mills, A.L., Hornberger, G.M., Herman, J.S., 1999. Spatial distribution of deposited bacteria following miscible displacement experiments in intact cores. Water Resour. Res. 35, 1797–1807.

Bradford, S.A., Abriola, L.M., 2001. Dissolution of residual tetrachloroethylene in fractional wettability porous media: incorporation of interfacial area estimates. Water Resour. Res. 37, 1183–1195.

Bradford, S.A., Simunek, J., Bettahar, M., Tadassa, Y.F., van Genuchten, M.Th., Yates, S.R., 2005. Straining of colloids at textural interfaces. Water Resour. Res. 41. doi:10.1029/2004WR003675 Art. No. W10404.

Bradford, S.A., Simunek, J., Bettahar, M., van Genuchten, M.Th., Yates, S.R., 2003. Modeling colloid attachment, straining, and exclusion in saturated porous media. Environ. Sci. Technol. 37, 2242–2250.

Bradford, S.A., Simunek, J., Bettahar, M., van Genuchten, M.Th., Yates, S.R., 2006a. Significance of straining in colloid deposition: evidence and implications. Water Resour. Res. 42. doi:10.1029/2005WR004791 Art. No. W12S15.

Bradford, S.A., Simunek, J., Walker, S.L., 2006b. Transport and straining of *E. coli* O157:H7 in saturated porous media. Water Resour. Res. 42. doi:10.1029/2005WR4805 Art. No. W12S12.

Bradford, S.A., Torkzaban, S., Walker, S.L., 2007. Coupling of physical and chemical mechanisms of colloid straining in saturated porous media. Water Res. 41, 3012–3024.

Bradford, S.A., Yates, S.R., Bettahar, M., Simunek, J., 2002. Physical factors affecting the transport and fate of colloids in saturated porous media. Water Resour. Res. 38 (12). doi:10.1029/2002WR001340 Art No.1327.

Cherrey, K.D., Flury, M., Harsh, J.B., 2003. Nitrate and colloid transport through coarse Hanford sediments under steady state, variably saturated flow. Water Resour. Res. 39, 1165. doi:10.1029/2002WR001944.

Crist, J.T., McCarthy, J.F., Zevi, Y., Baveye, P., Throop, J.A., Steenhuis, T.S., 2004. Pore-scale visualization of colloid transport and retention in partly saturated porous media. Vadose Zone J. 3 (2), 444–450.

Crist, J.T., Zevi, Y., McCarthy, J.F., Throop, J.A., Steenhuis, T.S., 2005. Transport and retention mechanisms of colloids in partially saturated porous media. Vadose Zone J. 4, 184–195.

Cushing, R.S., Lawler, D.F., 1998. Depth filtration: fundamental investigation through three-dimensional trajectory analysis. Environ. Sci. Technol. 32, 3793–3801.

de Jonge, H., Jacobsen, O.H., de Jonge, L.W., Moldrup, P., 1998. Particle-facilitated transport of prochloraz in undisturbed sandy loam soil columns. Soil Sci. Soc. Am. J. 27, 1495–1503.

de Jonge, L.W., Kjaergaard, C., Moldrup, P., 2004. Colloids and colloid-facilitated transport of contaminants in soils: An introduction. Vadose Zone J. 3, 321–325.

DeNovio, N.M., Saiers, J.E., Ryan, J.N., 2004. Colloid movement in unsaturated porous media. Recent advances and future directions. Vadose Zone J. 3, 338–351.

Derjaguin, B.V., 1954. Theory of the stability of strongly charged lyophobic sols and of the adhesion of strongly charged particles in solutions of electrolytes, Acta Physicochim. USSR 14, 733–762.

Elimelech, M., Nagai, M., Ko, C.H., Ryan, J.N., 2000. Relative insignificance of mineral grain zeta potential to colloid transport in geochemically heterogeneous porous media. Environ. Sci. Technol. 34, 2143–2148.

Gargiulo, G., Bradford, S.A., Simunek, J., Ustohal, P., Vereecken, H., Klumpp, E., 2007. Bacteria transport and deposition under unsaturated conditions: the role of the matrix grain size and the bacteria surface protein. J. Contam. Hydrol. 92, 255–273.

Gracia, A., Morel, G., Saulner, P., Lachaise, J., Schechter, R.S., 1995. The z-potential of gas bubbles. J. Coll. Interf. Sci. 172, 131–136.

Gregory, J., 1981. Approximate expression for retarded van der Waals interaction. J. Coll. Interf. Sci. 83, 138–145.

Harvey, R.W., Harms, H., 2002. Use of microorganisms and microspheres as tracers in groundwater. In: Britton, G. (Ed.), Encyclopedia of Environmental Microbiology. John Wiley & Sons, New York, pp. 3194–3202.

Herzig, J.P., Leclerc, D.M., LeGoff, P., 1970. Flow of suspension through porous media: application to deep filtration. Ind. Eng. Chem. Res. 62, 129–157.

Hoek, E.M.V., Agarwal, G.K., 2006. Extended DLVO interactions between spherical particles and rough surfaces. J. Coll. Interf. Sci. 298, 50–58.

Hogg, R., Healy, T.W., Fuerstenau, D.W., 1966. Mutual coagulation of colloidal dispersions. Trans. Faraday Soc. 62, 1638–1651.

Hurst, C.J., 1980. Survival of enteroviruses in rapid-infiltration basins during the land application of waste-water. Appl. Environ. Microbiol. 40, 192–200.

Israelachvili, J.N., 1992. Intermolecular and surface forces, 2nd ed. Academic Press, London.

Johnson, W.P., Li, X.Q., Yal, G., 2007. Colloid retention in porous media: mechanistic confirmation of wedging and retention in zones of flow stagnation. Environ. Sci. Technol. 41, 1279–1287.

Johnson, P.R., Elimelech, M., 1995. Dynamics of colloid deposition in porous media: blocking based on random sequential adsorption. Langmuir 11, 801–812.

Kuznar, Z.A., Elimelech, M., 2007. Direct microscopic observation of particle deposition in porous media: role of the secondary energy minimum. Coll. Surf. A: Physicochem. Eng. Aspects 294, 156–162.

Lenhart, J.J., Saiers, J.E., 2002. Transport of silica colloids through unsaturated porous media: experimental results and model comparisons. Environ. Sci. Technol. 36, 769–777.

Li, C., Somasundaran, P., 1991. Reversal of bubble charge in multivalent inorganic salt solutions—effect of magnesium. J. Coll. Interf. Sci. 146, 216–218.

Li, X., Lin, C.-L., Miller, J.D., Johnson, W.P., 2006. Pore-scale observation of microsphere deposition at grain-to-grain contacts over assemblage-scale porous media domains using X-ray microtomography. Environ. Sci. Technol. 40, 3762–3768.

Li, X., Scheibe, T.D., Johnson, W.P., 2004. Apparent decreases in colloid deposition rate coefficient with distance of transport under unfavorable deposition conditions: a general phenomenon. Environ. Sci. Technol. 38 (21), 5616–5625.

Marquardt, D.W., 1963. An algorithm for least-squares estimation of non-linear parameters. J. Soc. Ind. Appl. Math. 11, 431–441.

McDowell-Boyer, L.M., Hunt, J.R., Sitar, N., 1986. Particle transport through porous media. Water Resour. Res. 22, 1901–1921.

McGechan, M.B., Lewis, D.R., 2002. Transport of particulate and colloid-sorbed contaminants through soil. Part 1: general principles. Biosyst. Eng. 83, 255–273.

Padilla, I.Y., Yeh, T.-C., Conklin, M.H., 1999. The effect of water content on solute transport in unsaturated porous media. Water Resour. Res. 35, 3303–3313.

Patzek, T.W., Kristensen, J.G., 2001. Shape factor and hydraulic conductance in noncircular capillaries II. Two-phase creeping flow. J. Coll. Interf. Sci., 236, 305–317.

Patzek, T.W., Silin, D.B., 2001. Shape factor and hydraulic conductance in noncircular capillaries I. One-phase creeping flow. J. Coll. Interf. Sci., 236, 295–304.

Powelson, D.K., Gerba, C.P., Yahya, M.T., 1993. Virus transport and removal in wastewater during aquifer recharge. Water Res. 27, 583–590.

Ramachandran, V., Fogler, H.S., 1999. Plugging by hydrodynamic bridging during flow of stable colloidal particles within cylindrical pores. J. Fluid Mech. 385, 129–156.

Redman, J.A., Grant, S.B., Olson, T.M., Estes, M.K., 2001. Pathogen filtration, heterogeneity, and potable reuse of wastewater. Environ. Sci. Technol. 35, 1798–1805.

Redman, J.A., Walker, S.L., Elimelech, M., 2004. Bacterial adhesion and transport in porous media: role of the secondary energy minimum. Environ. Sci. Technol. 38, 1777–1785.

Ryan, J.N., Elimelech, M., 1996. Colloid mobilization and transport in groundwater. Coll. Surf. A 107, 1–56.

Ryan, J.N., Illangasekare, T.H., Litaor, M.I., Shannon, R., 1998. Particle and plutonium mobilization in macroporous soils during rainfall simulations. Environ. Sci. Technol. 32, 476–482.

Saiers, J.E., Lenhart, J.J., 2003a. Ionic-strength effects on colloid transport and interfacial reactions in partially saturated porous media. Water Resour. Res. 39, 1256. doi:10.1029/2002WR001887.

Schafer, A., Ustohal, P., Harms, H., Stauffer, F., Dracos, T., Zehnder, A.J.B., 1998. Transport of bacteria in unsaturated porous media. J. Contam. Hydrol. 33, 149–169.

Schijven, J.F., Hassanizadeh, S.M., 2000. Removal of viruses by soil passage: overview of modelling, processes, and parameters. Crit. Rev. Environ. Sci. Technol. 30, 49–127.

Simunek, J., van Genuchten, M.Th., Sejna, M., 2005. The HYDRUS-1D software package for simulating the one-dimensional movement of water, heat, and multiple solutes in variably-saturated media —Version

3.0, HYDRUS software series 1. Department of Environmental Sciences, University of California Riverside, Riverside, CA. 240 pp.

Tipping, E., 1981. The adsorption of aquatic humic substances by iron oxides. Geochim. Cosmochim. Acta 45, 191–199.

Toride, N., Inoue, M., Leij, F.J., 2003. Hydrodynamic dispersion in an unsaturated dune sand. Soil Sci. Soc. Am. J. 67, 703–712.

Torkzaban, S., Hassanizadeh, S.M., Schijven, J.F., de Bruin, H.A.M., de Roda Husman, A.M., 2006a. Virus transport in saturated and unsaturated sand columns. Vadose Zone J. 5, 877–885.

Torkzaban, S., Hassanizadeh, S.M., Schijven, J.F., van den Berg, H.H.J.L., 2006b. Role of air–water interfaces on retention of viruses under unsaturated conditions. Water Resour. Res. 42, W12S14. doi:10.1029/2006WR004904.

Tufenkji, N., Elimelech, M., 2005b. Spatial distributions of *Cryptosporidium* oocysts in porous media: evidence for dual mode deposition. Environ. Sci. Technol. 39, 3620–3629.

Walker, S.L., Redman, J.A., Elimelech, M., 2004. Role of cell surface lipopolysaccharides in *Escherichia coli* K12 adhesion and transport. Langmuir 20, 7736–7746.

Wan, J., Tokunaga, T.K., 1997. Film straining of colloids in unsaturated porous media: conceptual model and experimental testing. Environ. Sci. Technol. 31, 2413–2420.

Wan, J., Wilson, J.L., 1994a. Visualization of the role of the gas–water interface on the fate and transport of colloids in porous media. Water Resour. Res. 30, 11–23.

Wan, J., Wilson, J.L., 1994b. Visualization of the role of the gas–water interface on the fate and transport of colloids in porous media. Water Resour. Res. 30 (1), 11–23.

Wan, J.M., Tokunaga, T.K., 2002. Partitioning of clay colloids at air–water interfaces. J. Coll. Interf. Sci. 247, 54–61.

Yoon, J.S., Germaine, J.T., Culligan, P.J., 2006. Visualization of particle behavior with a porous medium: mechanisms for particle filtration and retardation during downward transport. Water Resour. Res. 42, W06417. doi:10.1029/2004WR003660.

Xu, S., Gao, B., Saiers, J.E., 2006. Straining of colloidal particles in saturated porous media. Water Resour. Res. 42, W12S16. doi:10.1029/2006WR004948.

Zevi, Y., Dathe, A., McCarthy, J.F., Richards, B.K., Steenhuis, T.S., 2005. Distribution of colloid particles onto interfaces in partially saturated sand. Environ. Sci. Technol. 39, 7055–7064.